Failed Escape: Solid Surfaces Prevent Tumbling of *Escherichia coli*

Mehdi Molaei,[1] Michael Barry,[2] Roman Stocker,[2] and Jian Sheng[1,*]
[1]*Mechanical Engineering Department, Texas Tech University, 2703 7th Street, Lubbock, Texas 79409, USA*
[2]*Ralph M. Parsons Laboratory, Department of Civil and Environmental Engineering, Massachusetts Institute of Technology, 15 Vassar Street, Cambridge, Massachusetts 02139, USA*
(Received 24 December 2013; published 7 August 2014)

Understanding how bacteria move close to surfaces is crucial for a broad range of microbial processes including biofilm formation, bacterial dispersion, and pathogenic infections. We used digital holographic microscopy to capture a large number ($> 10^3$) of three-dimensional *Escherichia coli* trajectories near and far from a surface. We found that within 20 μm from a surface tumbles are suppressed by 50% and reorientations are largely confined to surface-parallel directions, preventing escape of bacteria from the near-surface region. A hydrodynamic model indicates that the tumble suppression is likely due to a surface-induced reduction in the hydrodynamic force responsible for the flagellar unbundling that causes tumbling. These findings imply that tumbling does not provide an effective means to escape trapping near surfaces.

DOI: 10.1103/PhysRevLett.113.068103 PACS numbers: 47.63.Gd, 42.40.−i, 82.70.Dd, 87.64.M−

The motility of bacteria near surfaces is relevant in a broad range of applications, from biofilm formation on medical instruments and wounds [1], to biofouling of engineered surfaces [2], and bioremediation of pollutants in the environment [3,4]. The presence of surfaces is known to alter bacterial motility by inducing circular swimming trajectories [5,6] and trapping cells in the near-surface region [7–12]. These near-surface behaviors have been attributed to long-range hydrodynamic interactions between swimming bacteria and the nearby surface [5,7–13]: the surface modifies velocity and pressure fields around a swimming cell, and consequently forces and torques on the cell. Surfaces can also interfere with motility through steric interactions. For phytoplankton and spermatozoa, direct interaction of flagella with the surface is an important driver of surface scattering [14]. For smaller bacterial cells, measurements of the flow field around individual swimmers [15] indicate that hydrodynamic interactions are weak, suggesting that physical contact is critical in determining cell-surface interactions.

Efforts to understand the trapping of bacteria by surfaces have largely neglected the effect of tumbles, the reorientations exhibited by wild-type peritrichous bacteria in their swimming trajectories. Studies have focused instead on smooth-swimming mutants for a range of species, including *Escherichia coli* [6,7,9,15,16], *Caulobacter crescentus* [17], and *Bacillus subtilis* [18]. When tumbling has been considered, in the context of surface interactions in *E. coli*, it was suggested to act as a mechanism that favors the cells' escape from the near-surface region [7,19]. However, subsequent observations have shown that wild-type (i.e., tumbling) *E. coli* attach to surfaces as effectively as a smooth-swimming mutant [20]. This inconsistency highlights the current limitations in our understanding of the surface interactions of bacteria. Here, we describe the effect of a surface on wild-type *E. coli*, and specifically on its ability to tumble, by capturing three-dimensional swimming trajectories of thousands of individual cells in a microfluidic device. We discovered that tumbles are suppressed by 50% within 20 μm from the surface, indicating that tumbling does not provide an effective means to overcome trapping by the surface.

We applied digital holographic microscopy (DHM [21]) to track swimming bacteria in three dimensions. Bacteria are considerably more difficult to image with DHM compared to other objects previously imaged with this method, including larger plankton cells [22] and polystyrene spheres [23,24], due to their minute size and small contrast of the refractive index ($n = 1.35$) compared to that of water ($n = 1.33$). Following a careful optimization of the imaging optics, we succeeded in using DHM to simultaneously image up to ~3000 wild-type *E. coli* bacteria over the entire 200 μm depth of a microfluidic device, with a spatial resolution of 0.2 μm (lateral) and 0.5 μm (axial). By enabling simultaneous tracking of a large number of cells without any moving parts in the setup, this approach establishes DHM as a powerful technique for tracking bacteria *vis-á-vis* previous methods, including 3D tracking microscopy [25], scanning confocal microscopy, and 3D partial coherent tomographic digital holography [26].

The steady-state distribution of cells over the depth y of the microfluidic channel (Fig. 1) revealed that wild-type *E. coli* (strain AW405) were at least as strongly trapped near the top and bottom surfaces as a previously studied smooth-swimming mutant (strain HCB-437; [9]), for identical culturing conditions ([27,28]). Our experiments were performed within a straight polydimethylsiloxane (PDMS) microchannel, 45 mm long, 200 μm deep, and 5 mm wide, attached to a glass slide. We imaged a $400 \times 200 \times 400$ μm^3 volume within a midlogarithmic phase (optical density$_{600}$ = 0.45) suspension of cells by recording 15 holograms per

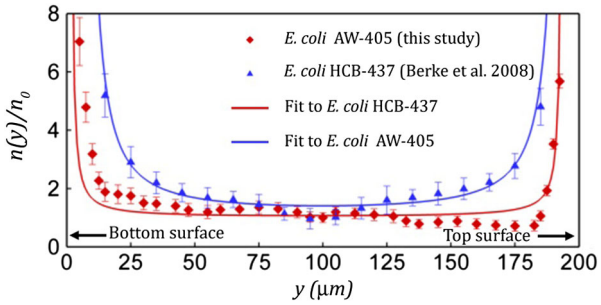

FIG. 1 (color online). Concentration of *E. coli* as a function of distance from the bottom surface y. Red diamonds and blue triangles indicate DHM measurements for wild-type strain AW405 and previous measurements for the smooth-swimming mutant strain HCB-437 [9], respectively. Solid curves are best fits based on the model $\frac{n(y)}{n_0} = \exp[L_\perp(\frac{1}{y} + \frac{1}{H-y})]$, where $H = 200$ μm is the channel depth, n_0 is the cell concentration in the bulk, and $L_\perp$ is the characteristic accumulation length scale. Best fits yielded $L_\perp = 5.1$ and 26.5 μm for the strains AW405 and HCB-437, respectively. In AW405 experiments, the top and bottom surfaces were made of PDMS and glass, respectively, whereas in strain HCB-437 experiments both were glass. Error bars denote standard deviations.

second for one minute with a 2048×2048 pixel CCD camera and a 40× objective (NA = 0.65). For each hologram, images at different depths were reconstructed numerically and in-focus images of individual bacteria were identified and used to compute bacterial positions [22]. The location of a surface was determined by the loci of bacteria immobilized on it, with a precision of 2 μm. The concentration profile $n(y)$ for *E. coli* strain AW405 (Fig. 1) is well predicted by a previously proposed model [9] and reveals an even tighter accumulation near the surfaces compared to strain HCB-437 (accumulation length $L_\perp = 5$ μm compared to 26 μm; see caption of Fig. 1). The asymmetry in the concentration profile of strain AW405 is a robust feature of our experiments (see [28]) and likely originates from the differences in surface properties of glass (bottom surface) and PDMS (top surface) (for comparison, the earlier experiments with *E. coli* strain HCB-437 were done in a system where both top and bottom were made of glass [9] and the associated profile is symmetric). The strong near-surface trapping of wild-type *E. coli* demonstrates that the ability to tumble does not aid *E. coli* in escaping from surfaces. In the following, we present a detailed analysis of swimming trajectories to determine the origin of this failed escape.

A collection of three-dimensional cell trajectories obtained with DHM is shown in Fig. 2(a). In the absence of stimuli and nearby surfaces, *E. coli* swims by alternating nearly straight runs and brief tumbles [40]. This was also the predominant swimming pattern we observed in the bulk [Fig. 2(b); 70% of total trajectory time in the bulk], defined as the region that is further than 20 μm from both the top and bottom surfaces (i.e., 20 μm $< y <$ 180 μm). We identified tumbles as rapid changes in swimming direction concomitant with rapid reductions in swimming speed, using identical criteria as in Berg and Brown's original experiments with a tracking microscope ([25,28]), and our statistics of the run-and-tumble motility pattern in the bulk agree closely with theirs (Table I). In particular, the mean swimming speed (14 μm/s) and the mean run time in the bulk ($T_b = 0.93$ s) differed by $< 1\%$ and ~8%, respectively, from those in [25]. Motility near surfaces was dramatically different [Figs. 2(d)–(g)]. The majority of cells within 20 μm from either surface (near-surface region) were loosely attached and gyrating on the surface [Fig. 2(d); 63% of total trajectory time in the near-surface region] or were in the process of attaching or detaching [Fig. 2(e); 11%]. Here we focus, however, on the swimming fraction of cells in this near-surface region (26%). Of these, many swam in a run-and-tumble pattern [Fig. 2(f); 19%], whereas a smaller percentage swam in circles [Fig. 2(g); 7%], a pattern known to result from a hydrodynamic torque caused by the proximity of the surface [6].

Identification of tumbles revealed a 50% reduction of tumbles in the near-surface region compared to the bulk. Whereas the mean swimming speed during runs was only 9% faster than that in the bulk (Table I), in agreement with previous numerical predictions of a ~10% increase [8], the run times in the near-surface region ($T_s = 1.94 \pm 1.96$ s; 2846 runs) were on average twice as long as those in the bulk ($T_b = 0.93 \pm 1.32$ s; 9619 runs) [Table I, Fig. 3(b)]. A t test indicates that T_s and T_b are statistically different at a 99.5% significance level (t score: 25.8). The probability density of the run time in the near-surface region peaked at 0.6 s and displayed a pronounced tail compared to that in the bulk, which peaked at 0.3 s and had a shorter tail [Fig. 3(b)]. Over 41% of near-surface runs lasted longer than twice the mean run time in the bulk ($2T_b = 1.86$ s) in contrast to only 16% of runs in the bulk. Run time characteristics [Fig. 3(b)] were estimated using an exponential distribution model [25,41]. Mean tumbling frequencies were approximated by finding e-folding time scales through best fits, yielding 1.3 tumbles/s in the bulk and 0.5 tumbles/s in the near-surface region. The tumble frequency in the bulk agrees well with 1.2 tumbles/s reported previously [25,41]. Finally, while bacteria could not be consistently tracked for times sufficient to measure the change in run time along a single trajectory for all measurements, this was possible in selected cases. Figure 3(a) (inset) shows a long trajectory of a cell that arrived at the surface from the bulk, distinctly reducing its tumbling frequency in the near-surface region.

The surface's quenching effect on tumbles extended 20 μm into the fluid. This was determined by computing the mean run time at different distances from the surface. The run time peaked at the surface and regressed to the value in the bulk over 20 μm [Fig. 4(a)]. This pattern is confirmed by direct quantification of tumbles as a function of distance (see the Supplemental Material [28], Fig. S3).

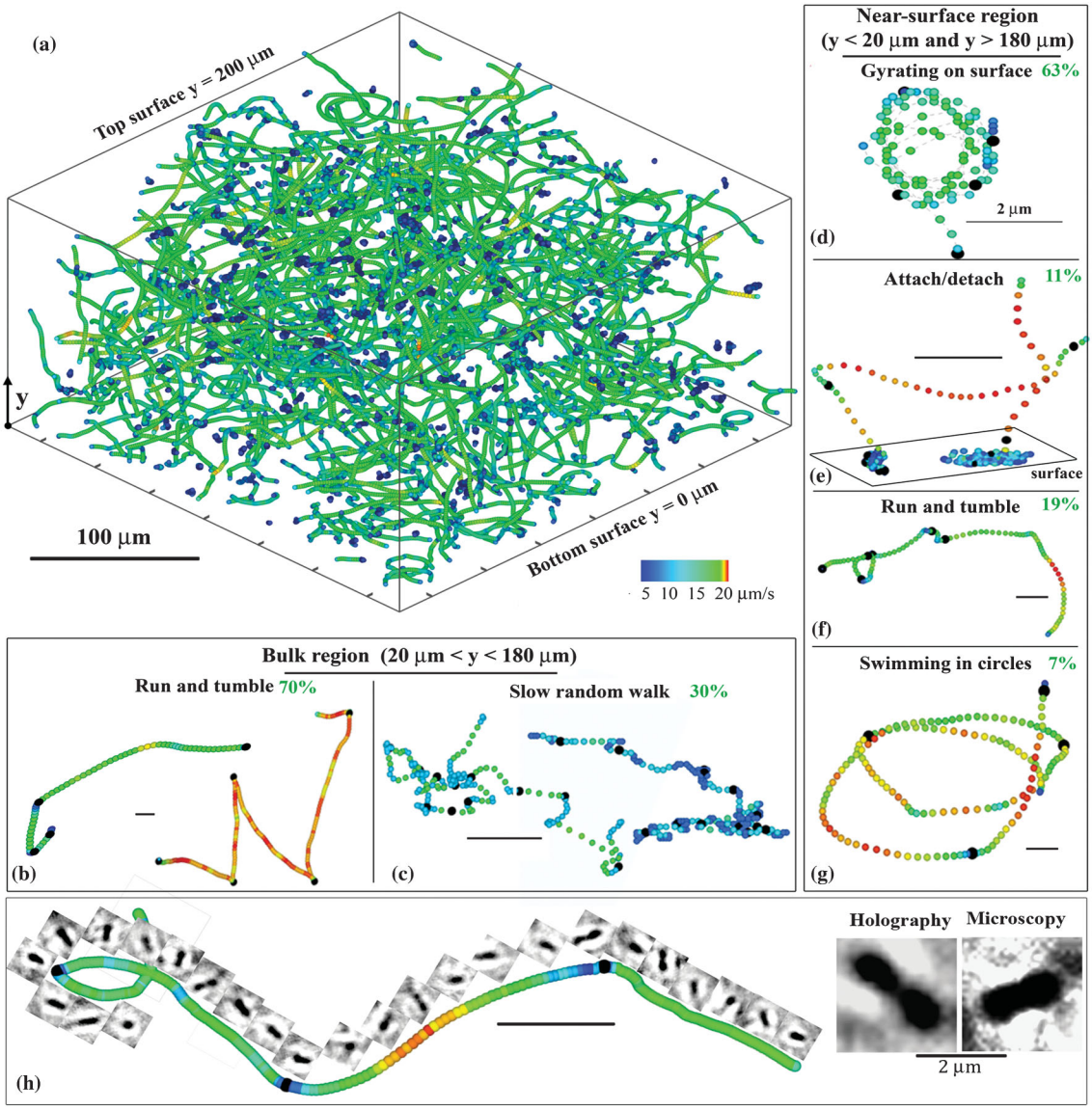

FIG. 2 (color). Gallery of three-dimensional swimming trajectories of wild-type *E. coli* (strain AW405). (a) Sample of 594 trajectories within a $400 \times 200 \times 400$ μm^3 volume. The surfaces are located at $y = 0$ (bottom) and 200 μm (top). (b)–(c) Sample trajectories in the bulk ($20 < y < 180$ μm) illustrate two motility patterns: (b) run-and-tumble and (c) a slow random walk. (d)–(g) Sample trajectories in the near-surface region (i.e., within 20 μm from either surface) illustrate cells (d) gyrating while attached, (e) attaching or detaching, (f) performing run-and-tumble, and (g) swimming in circles. Percentiles indicate the fraction of total trajectory time belonging to each motility pattern. (h) Sample trajectory showing the in-focus reconstructed bacterial image every seven frames (0.46 s). Inset: left, a reconstructed holographic in-focus image; right, a bright field micrograph obtained at 40×. Color code: swimming speed. Black circles: tumble events. Scale bar: 5 μm unless otherwise indicated.

This motivated our choice of 20 μm as the length scale separating the near-surface region from the bulk region. We note that 20 μm corresponds to twice the full length L_C of a bacterium inclusive of flagella.

Cells near the surface not only performed fewer tumbles, but also underwent much milder reorientations during tumbles, and these reorientations were skewed towards the surface-parallel direction. The tumbling angle (the change in direction between two consecutive runs) was on average 34% smaller in the near-surface region compared to the bulk (Table I). Furthermore, this reduction was strongly anisotropic, as reorientations towards the surface-normal direction were preferentially suppressed. This is manifest in the cosine of the swimming direction, θ (measured from the surface-normal direction), for new runs [Fig. 4(b)]. In the bulk, the probability density of $\cos\theta$ regresses to uniform [with a small deviation; Fig. 4(b), black line], as expected on theoretical grounds [Fig. 4(b), orange line], whereas it is increasingly more peaked in the surface-parallel direction ($\theta = 90°$) as the distance from the

TABLE I. Motility characteristics of wild-type *E. coli* in the bulk and near the surface compared to earlier results in the bulk [25]. The tumbling angle is the angle between two consecutive runs. D_{ii} $(i = x, y, z)$ are the dispersion coefficients along the three Cartesian directions (y is the surface-normal direction), computed from the autocorrelation of the Lagrangian swimming velocity [52]. $D = (D_{xx} + D_{yy} + D_{zz})/3$ is the mean dispersion coefficient and $A_{ii} = D_{ii}/D - 1$ measures dispersion anisotropy. Notice that the surface-normal dispersion (A_{yy}) is strongly suppressed in the near-surface region. Statistics were compiled over 2750 trajectories, excluding cells attached to or gyrating on surfaces [Fig. 2(d)], and represent mean ± standard deviation.

		Number of bacteria	Mean speed (μm/s)	Run time (s)	Tumbling angle (deg)	Dispersion, $D(10^{-9}$ m^2 s$^{-1})$	Dispersion anisotropy		
							A_{xx}	A_{yy}	A_{zz}
Berg and Brown [25]		35	14.2 ± 3.4	0.86 ± 1.18	68.0 ± 36.0	...	...	...	...
This study	In bulk	2194	14.1 ± 8.0	0.93 ± 1.32	71.3 ± 44.0	0.2	−0.03	−0.14	0.17
	Near surface	556	15.3 ± 6.8	1.94 ± 1.96	46.7 ± 39.1	0.14	0.57	−0.93	0.36

surface diminishes. In the following, we include both top and bottom surfaces in the analysis, and define $\tilde{h}$ as the distance from the nearest surface. For a 10 μm thick layer centered at $\tilde{h} = 15$ μm (i.e., 10 μm $< y <$ 20 μm and 180 μm $< y <$ 190 μm), a narrow peak in the distribution of $\cos\theta$ [width ~10°; Fig. 4(b)] around $\theta = 90°$ indicates a strong suppression of new surface-normal runs and a strong bias towards swimming parallel to the surface. Preferential surface-parallel motility is also supported by the large anisotropy in the dispersion coefficients computed from cell trajectories (Table I; method refers to the Supplemental Material [28]). These results help explain the surface-trapping of strain AW405 (Fig. 1) and demonstrate that their ability to tumble in bulk fluid is not an effective escape mechanism from surfaces, because tumbles near surfaces are strongly suppressed and runs occur primarily along the surface-parallel direction.

What is the mechanism by which a surface hinders tumbling? Steric hindrance, i.e., physical contact of the cell with the surface, has been proposed as the primary mechanism of surface scattering for eukaryotic cells including phytoplankton and spermatozoa [15]. In contrast, our observation that the distance from the surface wherein tumbles are suppressed [20 μm; Fig. 4(a)] is twice as large as the length of the cell inclusive of the flagella L_C indicates that steric hindrance cannot be the only mechanism responsible for tumble suppression in bacteria, and points instead toward the importance of hydrodynamic interactions.

This hypothesis is supported by a mathematical model of bacteria-surface interactions based on long-range hydrodynamic forces [25,28], which describes key flagellar processes during a run-tumble event. During a run, *E. coli*'s flagella bundle together and their rotation propels the cell forward. When one (or more) flagellar motor reverses the direction of rotation, viscous forces normal to the axes of the flagella cause them to move apart and unbundle [42,43] and the torque associated with this process reorients the cell, producing a tumble. We model this unbundling using a two-flagellum model, with a thicker flagellum representing the bundle rotating counterclockwise and a thinner flagellum representing the unbundling flagellum rotating clockwise (see the Supplemental Material [28], Fig. S4). In the bulk, the model produces radial forces that cause the two flagella to drift apart and unbundle. In contrast, near the surface the additional force singularities required to satisfy boundary conditions [12,25,28,44] have the effect of reducing the radial forces responsible for unbundling, thus quenching tumbles. When the quenching is strong enough, it leads to merging of consecutive runs and causes the elongation of mean run time. The model predicts that the run time T decreases with distance $\tilde{h}$ from the surface as $T/T_b = 1 + 0.39L_C/\tilde{h}$, in good agreement with experimentally measured run times [Fig. 4(a)], which a least-squares fit gives as $T/T_b = 0.99 + 0.37L_C/\tilde{h}$. This agreement further suggests that tumble suppression is a passive process outside the control of the cell, although this

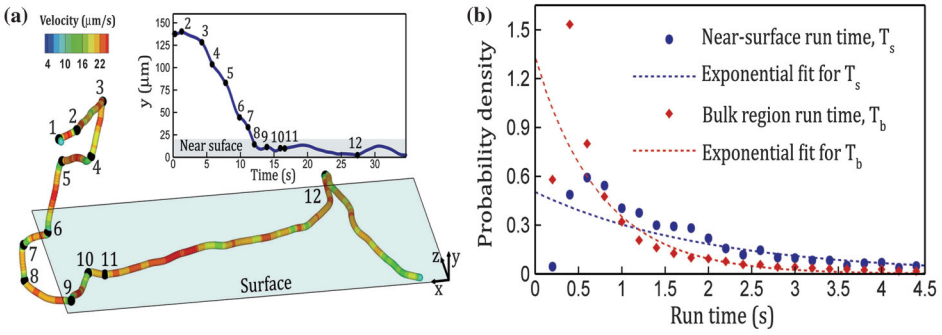

FIG. 3 (color). Surfaces suppress tumbling, resulting in longer run times. (a) Trajectory of a cell as it approaches the surface from the bulk. Black dots and numbers: tumble events. Inset: time series of the distance of the cell from the surface, showing approach from the bulk. (b) Probability density of run time in the bulk, T_b (red diamonds), and in the near-surface region T_s (blue circles). Dashed curves are exponential fits as done in [25].

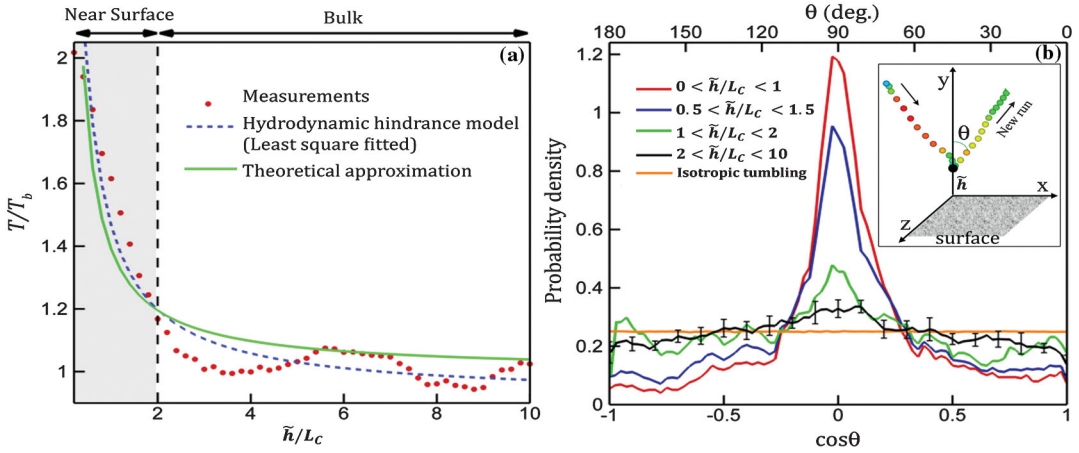

FIG. 4 (color). Tumbling and surface-normal motility are quenched within 20 μm from the surface. (a) Mean run time T at different distances from the surface $\tilde{h}$ relative to the mean run time in the bulk T_b. To include both surfaces, we used the distance $\tilde{h}$ from the nearest surface (bottom: $\tilde{h} = y$; top: $\tilde{h} = 200\,\mu\text{m} - y$). $L_C = 10$ μm is the approximate length of a bacterium inclusive of the flagella. Red circles: DHM measurements averaged over 5 μm thick, surface-parallel layers (see [25,28]). Blue dashed line: $T/T_b = 0.99 + 0.37L_c/\tilde{h}$, predicted from a model of near-surface swimming, with coefficients obtained by best fits. Green solid line: $T/T_b = 1 + 0.39L_c/\tilde{h}$ with coefficients derived theoretically ([25,28]). (b) Probability density (PD) of the cosine of the exit angle θ (the orientation of a new run immediately after a tumble), to the surface-normal direction (see inset). Data are shown for 10-μm thick, surface-parallel layers centered at $\tilde{h} = 5$, 10, and 15 μm. Also shown for reference is the mean PD measured in the bulk ($2 < \tilde{h}/L_c < 10$ or 20 μm $< y <$ 180 μm; black) and the calculated PD of an isotropic distribution of θ (orange). In the bulk, the mean PD in the bulk was obtained by averaging over the eight PDs obtained within 10-μm thick, surface-parallel layers ($2 < \tilde{h}/L_C < 3, \ldots, 9 < \tilde{h}/L_C < 10$). Error bars represent the standard deviation of the eight PDs.

of course does not exclude that cells may derive a fitness advantage from having tumbles suppressed and becoming trapped near surfaces (e.g., to facilitate biofilm formation). However, the proposed model can only predict qualitatively the trend of the observed bias of the tumbling angle, because the viscous resistance to flagella unbundling motion in the surface normal direction is expected to be greater than that in the surface parallel direction.

The ability to change swimming direction is a key component of bacterial motility, as it allows cells to exploit environmental cues (e.g., chemotaxis). Bacteria have evolved multiple strategies to reorient, including the nearly randomly oriented tumbles in peritrichous bacteria such as *E. coli*, *Salmonella typhimurium*, *Helicobacter pylori*, and *B. subtilis* [40,45,46], the reliance on Brownian reorientation during a stop of *Rhodobacter spheroides* [47], the swimming reversals of several uniflagellated bacteria including *C. crescentus* [48] and *Pseudomonas aeruginosa* [49], and the flick triggered by a buckling instability pervasive among uniflagellated marine bacteria [50,51]. Here we focused on *E. coli*'s tumbling, demonstrating that the frequency of occurrence of tumbles and the associated angular reorientations are greatly affected by solid surfaces (and, we speculate, other interfaces) that hinder *E. coli*'s migration away from the near-surface region. These results show that the strong effects of surfaces on the "run" component of *E. coli*'s motility [7] are compounded by additional, severe impacts on tumbles, with both processes acting to trap cells near surfaces. Whether other reorientation strategies are less sensitive to the influence of surfaces and can prevent surface trapping remains to be determined. Taken together, these findings underscore the powerful effects that surfaces exert on motile bacteria, fuel the current debate on whether bacteria-surface interactions have a hydrodynamic or steric origin, and call for a deeper understanding of how important microbial processes, including the initiation of biofilms and infections, depend on the physics of motility near surfaces.

Discussions with Thomas Powers are gratefully acknowledged. This work was supported by NIH Grant No. 1-R21-EB008844-01 (R. S. and J. S.), by NSF Grant No. CBET-1341901 (J. S.), and by NSF Grants No. OCE-0744641-CAREER and No. CBET-1066566 (R. S.).

*Corresponding author.
jian.sheng@ttu.edu

[1] T. Dalton, S. E. Dowd, R. D. Wolcott, Y. Sun, C. Watters, J. A. Griswold, K. P. Rumbaugh, and J. L. Herrmann, PLoS One **6** (2011).
[2] D. M. Yebra, S. Kiil, and K. Dam-Johansen, Prog, Organic Coatings **50**, 75 (2004).
[3] J. D. Kessler *et al.*, Science **331**, 312 (2011).
[4] D. Valentine *et al.*, Science **330**, 208 (2010).
[5] R. Di Leonardo, D. Dell'Arciprete, L. Angelani, and V. Iebba, Phys. Rev. Lett. **106**, 038101 (2011).
[6] E. Lauga, W. R. DiLuzio, G. M. Whitesides, and H. A. Stone, Biophys. J. **90**, 400 (2006).

[7] P. D. Frymier, R. M. Ford, H. C. Berg, and P. T. Cummings, Proc. Natl. Acad. Sci. U.S.A. **92**, 6195 (1995).
[8] M. Ramia, D. L. Tullock, and N. Phanthien, Biophys. J. **65**, 755 (1993).
[9] A. P. Berke, L. Turner, H. C. Berg, and E. Lauga, Phys. Rev. Lett. **101**, 038102 (2008).
[10] Y. Magariyama, M. Ichiba, K. Nakata, K. Baba, T. Ohtani, S. Kudo, and T. Goto, Biophys. J. **88**, 3648 (2005).
[11] H. Shum, E. A. Gaffney, and D. J. Smith, Proc. R. Soc. A **466**, 1725 (2010).
[12] S. E. Spagnolie and E. Lauga, J. Fluid Mech. **700**, 105 (2012).
[13] E. Lauga and T. R. Powers, Rep. Prog. Phys. **72**, 096601 (2009).
[14] V. Kantsler, J. Dunkel, M. Polin, and R. E. Goldstein, Proc. Natl. Acad. Sci. U.S.A. **110**, 1187 (2013).
[15] K. Drescher, J. Dunkel, L. H. Cisneros, S. Ganguly, and R. E. Goldstein, Proc. Natl. Acad. Sci. U.S.A. **108**, 10940 (2011).
[16] L. Lemelle, J.-F. Palierne, E. Chatre, and C. Place, J. Bacteriol. **192**, 6307 (2010).
[17] G. Li, J. Bensson, L. Nisimove, D. Munger, P. Mahautmr, and J. X. Tang,, Phys. Rev. E **84**, 041932 (2011).
[18] Marcos, H. C. Fu, T. R. Powers, and R. Stocker, Proc. Natl. Acad. Sci. U.S.A. **109**, 4780 (2012).
[19] G. Li and J. X. Tang, Phys. Rev. Lett. **103**, 078101 (2009).
[20] J. W. McClaine and R. M. Ford, Appl. Environ. Microbiol. **68**, 1280 (2002).
[21] J. Sheng, E. Malkiel, and J. Katz, Appl. Opt. **45**, 3893 (2006).
[22] J. Sheng, E. Malkiel, J. Katz, J. E. Adolf, and A. R. Place, Proc. Natl. Acad. Sci. U.S.A. **107**, 2082 (2010).
[23] J. Sheng, E. Malkiel, and J. Katz, J. Fluid Mech. **633**, 17 (2009).
[24] J. Katz and J. Sheng, Annu. Rev. Fluid Mech. **42**, 531 (2010).
[25] H. C. Berg and D. A. Brown, Nature (London) **239**, 500 (1972).
[26] T.-W. Su, L. Xue, and A. Ozcan, Proc. Natl. Acad. Sci. U.S.A. **109**, 16018 (2012).
[27] J. Adler, J. Gen. Microbiol. **74**, 77 (1973).
[28] See Supplemental Material at http://link.aps.org/supplemental/10.1103/PhysRevLett.113.068103, which includes Refs. [29–39], for a summary of the methods used for culture preparation, experiment observations, and data analysis in Sec. S1. Section S2 provides the characteristics on the bulk swimming mode that differs from the well-known random-walk motility. The development of hydrodynamic model on tumbling suppression near a surface is described in great details in Sec. S3.
[29] J. Sheng, E. Malkiel, and J. Katz, Exp. Fluids **45**, 1023 (2008).
[30] J. Sheng, E. Malkiel, J. Katz, J. Adolf, R. Belas, and A. R. Place, Proc. Natl. Acad. Sci. U.S.A. **104**, 17512 (2007).
[31] J. Sheng, E. Malkiel, J. Katz, J. E. Adolf, R. Bekas, and A. R. Place, J. Phycol. **43**, 25 (2007).
[32] A. Chengala, M. Hondzo, and J. Sheng, Phys. Rev. E **87**, 052704 (2013).
[33] Y. Xia and G. M. Whitesides, Annu. Rev. Mater. Sci. **28**, 153 (1998).
[34] N. C. Darnton, L. Turner, S. Rojevsky, and H. C. Berg, J. Bacteriol. **189**, 1756 (2007).
[35] M. Kim and T. R. Powers, Phys. Rev. E **69**, 061910 (2004).
[36] J. Gray and G. J. Hancock, J. Exp. Biol. **32**, 13 (1955).
[37] M. J. Kim and T. R. Powers, Phys. Rev. E **69**, 061910 (2004).
[38] M. J. Kim, M. J. Kim, J. C. Bird, J. Park, T. R. Powers, and K. S. Breuer, Exp. Fluids **37**, 782 (2004).
[39] J. Lighthill, SIAM Rev. **18**, 161 (1976).
[40] H. C. Berg, *E. coli in Motion* (Springer, New York, 2004).
[41] S. A. Biondi, J. A. Quinn, and H. Goldfine, AIChE J. **44**, 1923 (1998).
[42] N. C. Darnton and H. C. Berg, Biophys. J. **92**, 2230 (2007).
[43] M. J. Kim, M. J. Kim, J. C. Bird, J. Park, T. R. Powers, and K. S. Breuer, Exp. Fluids **37**, 782 (2004).
[44] J. R. Blake and A. T. Chwang, J. Eng. Math. **8**, 23 (1974).
[45] R. Stocker, Proc. Natl. Acad. Sci. U.S.A. **108**, 2635 (2011).
[46] R. M. Stark, G. J. Gerwig, R. S. Pitman, L. F. Potts, N. A. Williams, J. Greenman, I. P. Weinzweig, T. R. Hirst, and M. R. Millar, Lett. Applied Microbiol. **28**, 121 (1999).
[47] T. Pilizota, M. T. Brown, M. C. Leake, R. W. Branch, R. M. Berry, and J. P. Armitage, Proc. Natl. Acad. Sci. U.S.A. **106**, 11582 (2009).
[48] G. Li, L.-K. Tam, and J. X. Tang, Proc. Natl. Acad. Sci. U.S.A. **105**, 18355 (2008).
[49] L. Pratt and R. Kolter, Mol. Microbiol. **30**, 285 (1998).
[50] L. Xie, T. Altindal, S. Chattopadhyay, and X.-L. Wu, Proc. Natl. Acad. Sci. U.S.A. **108**, 2246 (2011).
[51] K. Son, J. Guasto, and R. Stocker, Nat. Phys. **9**, 494 (2013).
[52] G. I. Taylor, Proc. London Math. Soc. **20**, 196 (1921).